Supporting Information

Friedman et al. 10.1073/pnas.1718635115

SI Methods

Measurements of Oxygen in the Intestinal Tissue and in the Gut Lumen of Mice. Oxygen concentration measurements were performed using the phosphorescence quenching method (10). For measurements of oxygen in the intestinal tissue, well-established hydrophilic phosphorescent probe Oxyphor G4 (12) was injected into the tail vein of a mouse, and the phosphorescence was excited locally by a laser focused on the intestinal compartment of interest (stomach, duodenum, cecum, etc.) in a spot ∼0.1 mm in diameter. The duration of each individual measurement was 0.2–0.5 s depending on the level of signal. Oxyphor G4 is a large hydrophilic molecule (12). When injected systemically in mice, it becomes distributed through the circulation within seconds and remains confined to the vasculature, while slowly (hours) diffusing into the interstitial space. Our measurements were performed within minutes after injection and therefore reflected on average capillary pO_2 in the intestinal tissue.

Water-soluble Oxyphors are not appropriate for oxygen measurements in the lumen, where they may interact with luminal contents, undergo unpredictable transformations during digestion, and as a result lose their ability to report on oxygen quantitatively. Instead, previously we have developed micrometer-scale phosphorescent particles (10–20 μm in diameter), where the phosphorescent dye molecules (Pt tetrabenzoporphyrin) were dissolved in a solid polymer matrix (10). Being highly hydrophobic, the porphyrin molecules are unable to leach out of the particles into the environment, remaining confined exclusively to the polymer. Due to the large micrometer-scale size of the particles (large volume/surface ratio), the immediate environment of nearly all oxygen-sensing chromophores is due to the polymer. Consequently, oxygen response of the particles (calibration) does not change regardless of the medium in which the particles are immersed, whether it is water, more viscous fluid, or semisolid luminal material. Of course, due to the large size, equilibration of the particle bulk with the outside oxygen takes longer time than in the case of molecular probes. Nevertheless, the particles' response time is still very short—that is, fractions of second.

Preparation and Calibration of Oxyphor MicroS. The orifices of injection tube and collection tube were 20 μm and 150 μm, respectively. The disperse phase was a solution of PMMA (approximate molecular weight = 75,000; Scientific Polymer Products, Inc.) 10 wt% dissolved in 1, 2-Dichloroethane (Fisher Science), with a small amount of Pd tetraaryltetrabenzoporphyrin (PdTBP) added as an oxygen-sensitive phosphorescence probe. The continuous phase was an aqueous solution of 2 wt% poly (vinyl alcohol) (PVA; 87–89% hydrolyzed, average M_w = 13,000–23,000; Sigma Aldrich) that served to stabilize the PMMA droplets. The disperse and continuous solutions were pumped into the device with flow rates of 700 μL/h and 15 mL/h, respectively; PMMA droplets (∼58 μm in diameter) were generated; and then the emulsion was discharged into a vacuum evaporator for ∼20 h. As the solvent evaporated, the droplets solidified to form PMMA spheres containing the phosphorescence probe.

Statistical Analyses of in Vitro Oxygen Consumption Results. To determine the differences in oxygen consumption between the groups, a linear regression model was fitted using log(time to anaerobic) as the response and group (e.g., conventionally housed mice, germ free), log(mass cecal contents), and starting oxygen levels (mmHg) as covariates. Each group was compared with conventionally housed cecal contents, and $P < 0.05$ was considered statistically significant.

Lipidomics. Optima grade methanol, water, acetonitrile, chloroform, and 2-propanol were from Fisher. Gasses were supplied by Airgas. Spin 0.22-μm nylon filters were from Corning Costar. LC vials were from Waters Corp.

Cecal homogenate was thawed at 4 °C, and a 50 μL aliquot was transferred to a 1.5 mL low retention Eppendorf tube containing 210 μL of ice-cold water with 40 ng [$^2H_2{}^{13}C_2$]-Cer-(d18:1/C18:0) (Avanti Polar Lipids) as an internal standard. We added 380 μL of methanol and 7,600 μL of $CHCl_3$, and the mixture was vortexed three times for 50 s each. The samples were then centrifuged at 8,000 × *g* for 10 min at 4 °C to separate the phases. The lower organic phase was transferred to a clean 1.5-mL low-retention Eppendorf tube. The sample was evaporated to dryness under nitrogen. The residue was resuspended in 200 μL isopropanol:acetonitrile:water (3:5:2 vol/vol/v). The sample was spun down, filtered through a 0.22-μm spin filter (nylon; CoStar) at 10,000 × *g* for 10 min at 4 °C, and transferred to a LC vial for ultra-performance liquid chromatography (UPLC)-MS analysis. We then made 3-μL injections.

LC separations were conducted as previously described (1) using a Waters nano-ACQUITY UPLC system (Waters Corp.). A Waters XBridge BEH130 C18 column (100 μm × 150 mm, 1.7 μm pore size; Waters Corp) was employed for metabolites separation. The flow rate was 1.6 μL/min; solvent A was water:acetonitrile (4:6 vol/vol) with 0.1% formic acid and 10 mM ammonium formate, and solvent B was acetonitrile:isopropanol (1:9 vol/vol) with 0.1% formic acid and 10 mM ammonium formate. The gradient was 32% B at 0 min, 32% B at 6 min, 60% B at 11 min, 60% B at 15 min, 80% B at 27 min, 80% B at 30 min, 85% at 35 min, 85% at 45 min, 30% at 47 min, and 30% B at 55 min. Separations were performed at 55 °C.

For LC–high-resolution mass spectrometry analysis, a recently calibrated QE Exactive hybrid mass spectrometer (Thermo Fisher) was used in positive ion mode with a heated electrospray ionization source. The operating conditions were as follows: spray voltage, 1.5 kV; capillary temperature, 200 °C; capillary voltage, 0 V; tube lens, 80 V.

A control extraction blank was made using 50 μL of water instead of the homogenate. Untargeted and bioinformatics analyses were conducted using SIEVE 2.1 (Thermo Fisher) and XCMS. To help exclude noise and artifacts of analysis, the threshold feature intensity was set at $1e10^5$ and mass spectral features with a $P > 0.01$ by Welch's unpaired *t* test were manually examined to confirm good chromatographic peak shapes. From these hits, an accurate mass database search was performed through LipidSearch, HMBD, METLIN, KEGG, and ChemSpider. Targeted peak integration was confirmed in Xcalibur.

Proteomics. Cecal extracts in water were added to 9 volumes of urea lysis buffer (8 M urea, 0.1 M NaCl, 25 mM Tris, pH 8) supplemented with protease and phosphatase inhibitors. Extracts were then sonicated on ice three times for 10 s (approx. 17 W output) with intervening 10-s rests. Insoluble debris was pelleted by centrifugation at 15,996 × *g* and 4 °C for 10 min in a microfuge. After assaying the supernatant for protein content, equivalent amounts of protein (10–20 μg) were reduced with 10 mM DTT for 30 min at 56 °C and then alkylated with 50 mM iodoacetamide for 40 min at room temperature in the dark. Subsequently, protein samples were diluted with 4 volumes of

50 mM Tris, pH 8, and digested with trypsin overnight at 37 °C at a 1:20 mass ratio. Digests were acidified and then desalted before analysis by MS.

Peptides were separated by an Easy nLC-1000 LC system (Thermo) through 75 μm i.d. × 20 cm fused silica columns (Polymicro Tech) packed in house with ReproSil-Pur 120 C18-AQ (3 μm; Dr. Maisch GmbH) eluting directly into an Orbitrap Elite (Thermo) mass spectrometer. Water and acetonitrile containing 0.1% formic acid served as solvents A and B, respectively. The chromatography gradient consisted of 2% B to 28% B over 90 min, 28% B to 85% B over 5 min, and 85% B for 10 min. Fourier transformed mass spectra were acquired in the orbitrap in positive profile mode over a range of 350–1,200 *m*/*z* at a resolution of 120,000. The top 10 most intense precursor ions were fragmented by collision-induced dissociation at a normalized collision energy of 35 and analyzed in the ion trap. After acquisition, spectra were searched against the mouse proteome with Proteome Discoverer software (Thermo), with a false discovery rate < 0.01. Carbamidomethylation (+57.021) at Cys; mono-oxidation (+15.995) at Met, Trp, and Phe; di-oxidation (+31.990) at Met, Cys, and Trp; trioxidation (+47.985) at Cys; and conversion of Trp to kynurenine (+3.995) were set as dynamic modifications. Data were exported to Microsoft Excel for further analysis.

Analysis of 16S-Tagged Sequencing and Copy Number PCR Results Shown in Fig. 4. To estimate the rate of bacterial oxygen consumption, shown in Fig. 4*C*, the number of 16S rRNA gene copies per gram material was divided by 1.5 copies per cell to obtain the approximate number of bacterial cells. This value was then multiplied by both the proportion of facultative anaerobes in the sample and the rate of oxygen consumption per facultative anaerobe cell, resulting in an estimate for oxygen consumption per gram per second. For the purposes of these calculations, bacteria were annotated as obligately anaerobic, facultatively anaerobic, or aerobic. The S24-7 family represents the greatest proportion of Bacteroidetes (37) and has been characterized as a family of obligate anaerobes by genome analysis (38) and culture (39). The greatest proportion of Firmicutes belongs to the Lachnospiraceae family, the Turicibacter genus, and the Ruminococcaceae family, which are all described as obligate anaerobes (40). A smaller portion of the Firmicutes were assigned as *Lactobacillus*, which are annotated as facultative anaerobes (40). The remaining Firmicutes were attributed to the Clostridiales order, *Clostridium* cluster XI (41), and the Oscillibacter genus, all known to be obligate anaerobes (40). Operational taxonomic units in the Proteobacteria phylum were primarily attributed to *Pseudomonas*, an aerobic bacterium (40). Collectively, these taxonomic groups represent over 90% of the 16S marker gene assignments and are displayed in Fig. S4.

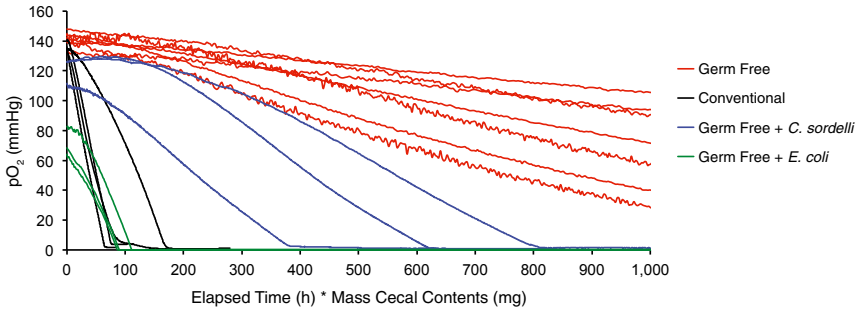

Fig. S1. In vitro oxygen consumption by cecal contents of conventionally housed and germ-free mice as well as cecal contents from germ-free mice inoculated with either *E. coli* or *C. sordelli* ($1.25–1.5 \times 10^9$ cfu/g cecal contents for *E. coli* and $1.75–2.15 \times 10^9$ cfu/g cecal contents for *C. sordelli*). The *x* axis (time) is adjusted to take into account the mass of the cecal contents. Statistical analysis by linear regression modeling: germ-free vs. conventional ($P < 0.001$); germ-free + *E. coli* vs. conventional (P = nonsignificant); germ-free + *C. sordelli* vs. germ-free ($P < 0.05$); germ-free + *C. sordelli* vs. conventional ($P < 0.05$).

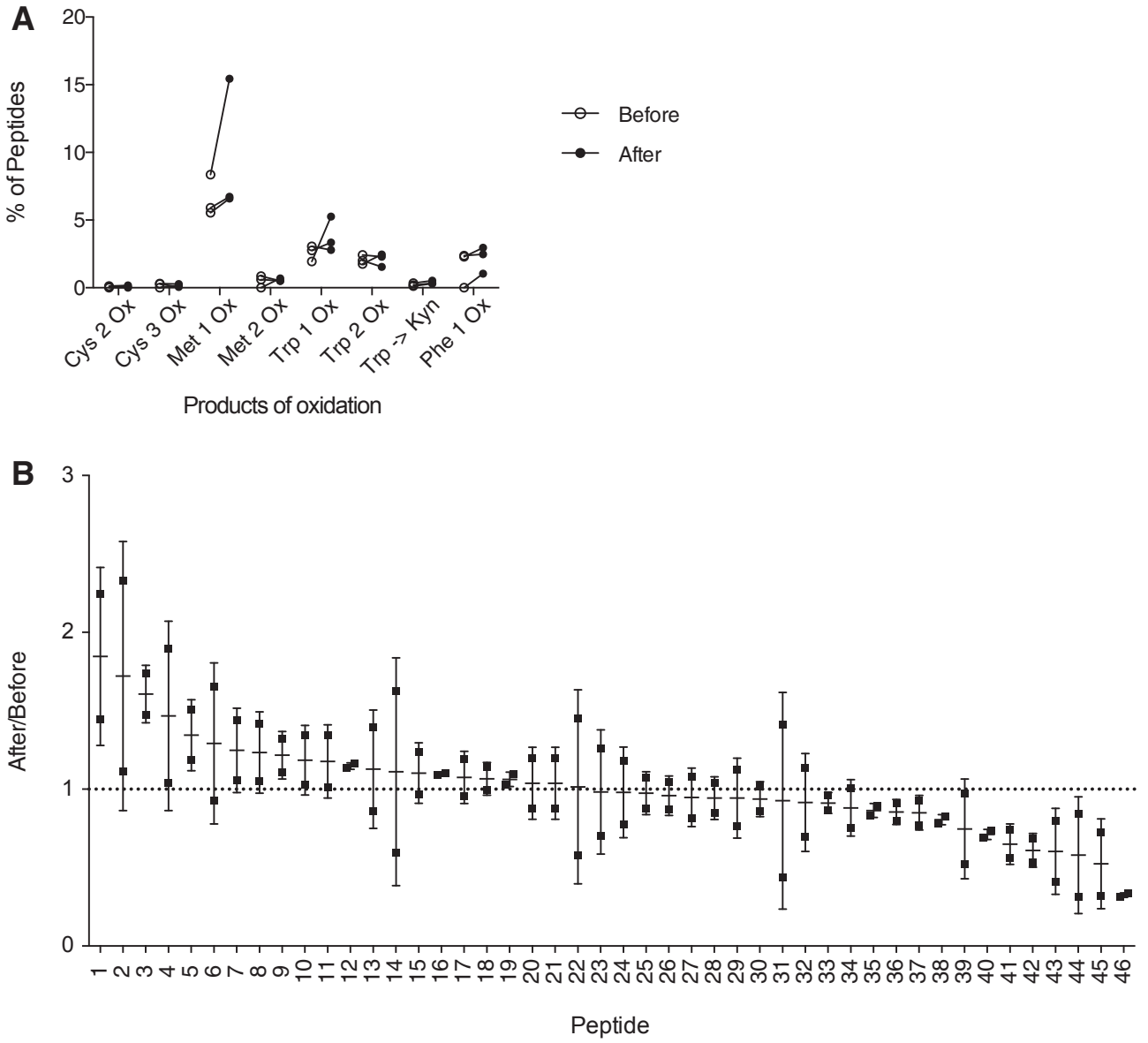

Fig. S2. Proteomic profiling of cecal contents from germ-free mice exposed to oxygen in vitro. (*A*) Protein extracts from the cecal material of germ-free mice were analyzed for oxidation products (mono-, di-, and trioxidation and conversion of tryptophan to kynurenine) at specific amino acid side chains by LC–MS/MS. The spectral count of each oxidized species as a percentage of total spectral counts is displayed before and after oxygen consumption for three paired biological replicates. Oxidation of methionine to sulfoxide and oxidation of tryptophan and phenylalanine are usually readily detectable, while the conversion of cysteine to an oxyacid, tryptophan to kynurenine, and methionine to a sulfone are less common. (*B*) The extracted ion chromatograms of 46 oxidized peptides were examined manually to calculate the relative abundance of the oxidized species based on the peak areas of both oxidized and nonoxidized forms of the peptides. The fold-change in the relative abundance of the oxidized species after oxygen consumption is plotted (mean ± SD from two paired biological replicates with two technical replicates).

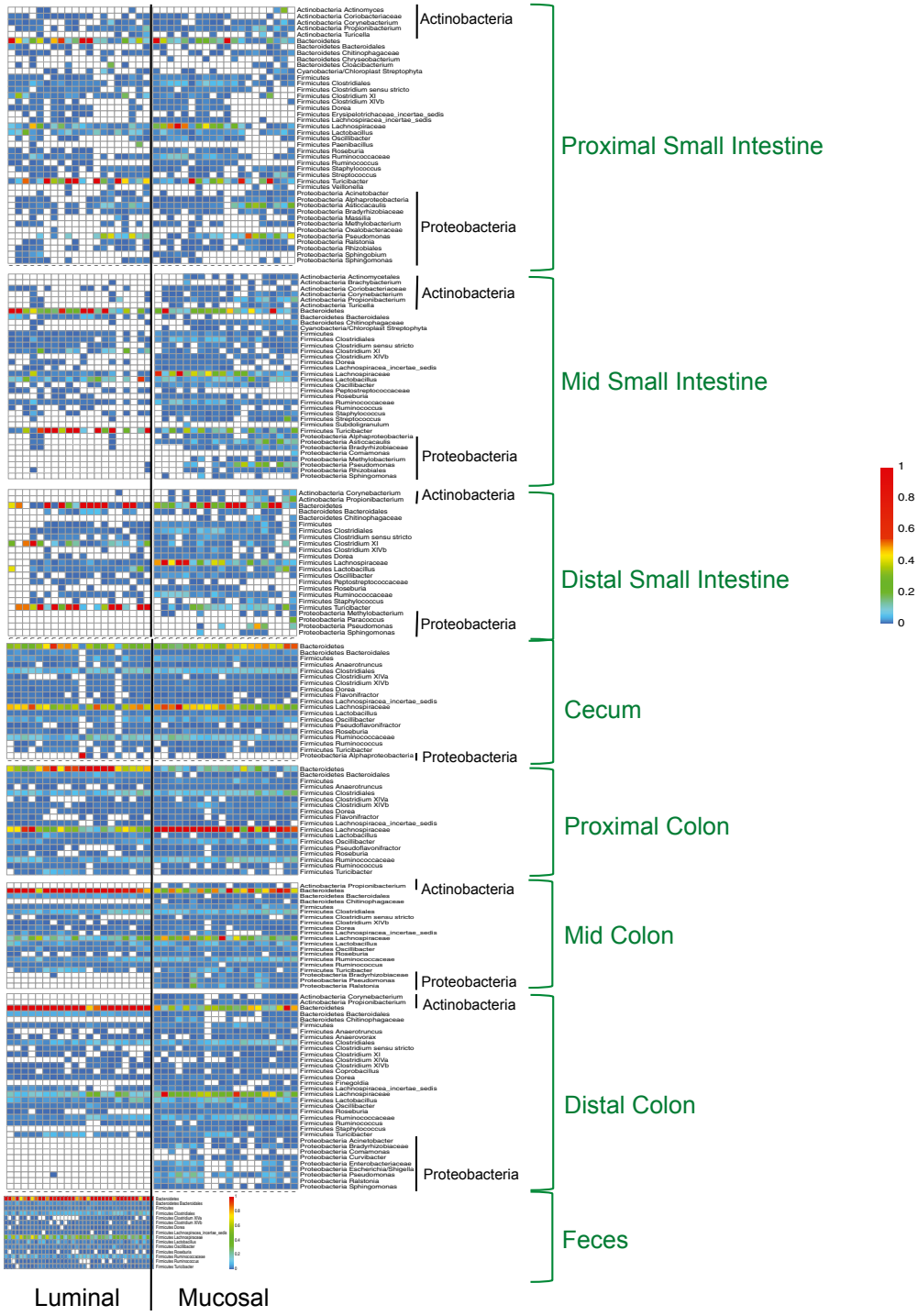

Fig. S3. Heatmap showing the taxonomic composition of bacteria in luminal and mucosal samples collected along the intestinal tract, as determined by 16S rRNA gene tag sequencing. Each column represents a different sample; each row represents a bacterial taxon; the color of each cell indicates relative abundance. Highlighted taxa fall within the Actinobacteria and Proteobacteria phyla.

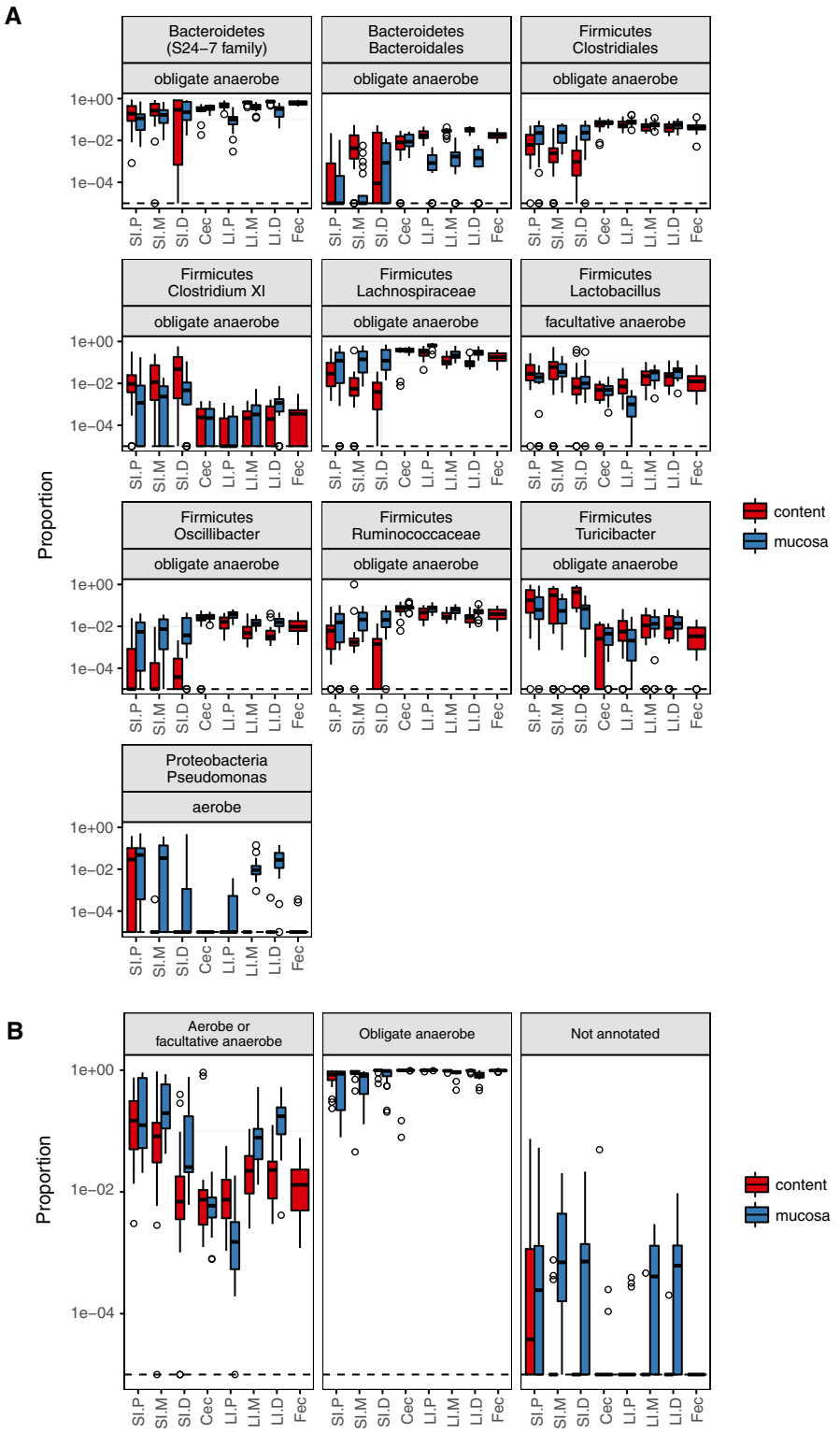

Fig. S4. Classification of bacteria along the intestinal tract as either obligately anaerobic or aerobe/facultative anaerobe. (*A*) Proportions of the top 10 bacterial taxa comprising the gut microbiota in luminal and mucosal samples throughout the length of the intestinal tract, as determined by 16S rRNA marker gene sequencing. (*B*) Total proportion of bacteria classified as aerobe/facultative anaerobe, obligate anaerobe, or not annotated with aerobic status.

Location	Proximal Small Intestine	Mid Small Intestine	Distal Small Intestine	Cecum	Proximal Large Intestine	Mid Large Intestine	Distal Large Intestine	Feces
Surface Area	++++	++++	+++++	+	+	+	+	N/A
Luminal diameter	+	+	+	++++	+	+	+	N/A
Liquid	++++	+++	+++	++	++	++	+	+
Prot. + Act: Mucosal/ Luminal:	17 17/17	14 14/3	6 6/0	1 1/1	0 0/0	4 4/0	9 9/0	0 0
Relative Bacterial Load	1X	18X	50X	1000X	1000X	1000X	1000X	1000X

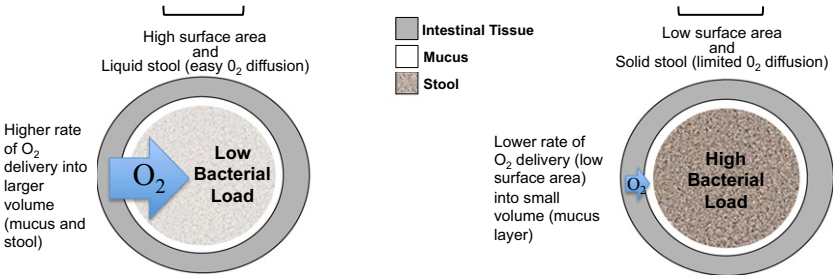

Fig. S5. A model for the relationship between the physical characteristics of the intestinal tract, its luminal contents, and the gut microbiota. (*Top*) Table describing the anatomic differences in the intestinal tract and liquid content of feces together with a summary of the abundance of Actinobacteria and Proteobacteria along the length of the intestinal tract. (*Bottom*) A conceptual diagram of the interaction between the host and the gut microbiota focused on oxygen diffusion and consumption in the proximal and distal intestinal tract.